N72-12161

APPLICATION OF THIN FILMS TO EXTREMELY HIGH FREQUENCIES

Final Report
on
NASA Grant NGR-47-005-001

Submitted by
Dr. Robert L. Ramey
Professor
Department of Electrical Engineering

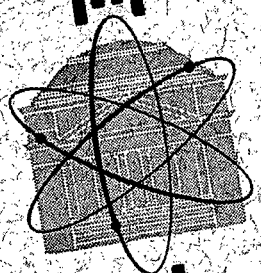

Research Laboratories for the Engineering Sciences

University of Virginia

Charlottesville

Report No. EE-4012-113-71U

July 1971

APPLICATION OF THIN FILMS TO EXTREMELY HIGH FREQUENCIES

Final Report
on
NASA Grant NGR-47-005-001

Submitted by
Dr. Robert L. Ramey
Professor
Department of Electrical Engineering

Department of Electrical Engineering
RESEARCH LABORATORIES FOR THE ENGINEERING SCIENCES
SCHOOL OF ENGINEERING AND APPLIED SCIENCE
UNIVERSITY OF VIRGINIA
CHARLOTTESVILLE, VIRGINIA

Report No. EE-4012-113-71U
July 1971

Copy No. _____

TABLE OF CONTENTS

LIST OF FIGURES

ABSTRACT

This report covers the final year of the thin film microwave research project which began December 5, 1967. In the summer of 1967 Ramey and Lewis demonstrated that the finite transmission of EM energy through thin films was practical. This was a verification of the work of Kaplan and also Korolev and Gridnev, all of the USSR. The subsequent research was based upon this phenomenon. The results of this research have been published extensively and several patent applications applied for. This last year of research (1970) was devoted primarily to application investigations. In particular, the use of thin film irises to control the beam direction from an array of microwave horns was explored with encouraging results.

SECTION I

INTRODUCTION

The possibility that electromagnetic radiation can pass through a conducting sheet is a plausible concept when we think of a skin depth

$$\delta = \sqrt{2/\omega\mu\sigma} \tag{1}$$

meters. For silver, at 10 GHz, the skin depth is 6.42×10^{-7} meters or 6420 angstrom units. Thin films of both metals and semiconductors can be produced as thin as several hundred angstroms before severe dislocation densities and occlusions begin to become a problem. Therefore it appears technically feasible to produce films through which detectable transmissions should be obtained. Equation (1) does not predict the transmission, thus a proper solution is required.

Kaplan, in the USSR, derived the expressions for the power transmission coefficient, T; the power reflection coefficient, R; and the power absorption coefficient, A; for the case of a plane TEM wave incident upon a thin metal film. Limited verification of Kaplan's theory was obtained by Korlev and Gridnev[2] also of the USSR, in 1965. In the summer of 1967 Ramey and Lewis[3] at the University of Virginia made successful measurements of the three power coefficients for a TE wave at 9.8 GHz for conducting films mounted in the transverse plane of rectangular waveguide, (see Fig. 1). They showed that the power transmission coefficient is given by

$$T = \left|\frac{E_3}{E_0}\right|^2 = \left|\frac{4e^{\gamma d}}{(1-\mu\gamma_2/\mu_2\gamma)(1-\mu_2\gamma/\mu\gamma_2)\exp(-\gamma_2 d)+(1+\mu\gamma_2/\mu_2\gamma)(1+\mu_2\gamma/\mu\gamma_2)\exp(\gamma_2 d)}\right|^2 \tag{2}$$

and the power-reflection coefficient is:

$$R = \left|\frac{E_1}{E_0}\right|^2 = \left|\frac{(1-\mu\gamma_2/\mu_2\gamma)(1+\mu_2\gamma/\mu\gamma_2)+(1+\mu\gamma_2/\mu_2\gamma)(1-\mu_2\gamma/\mu\gamma_2)\exp(-2\gamma_2 d)}{(1+\mu\gamma_2/\mu_2\gamma)(1+\mu_2\gamma/\mu\gamma_2)+(1-\mu\gamma_2/\mu_2\gamma)(1-\mu_2\gamma/\mu\gamma_2)\exp(-2\gamma_2 d)}\right|^2 \tag{3}$$

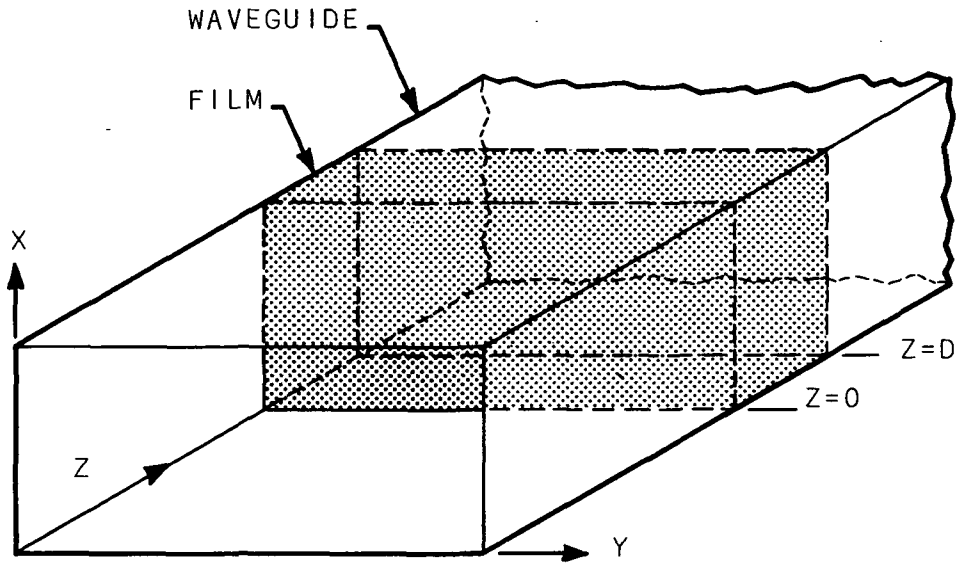

(A)

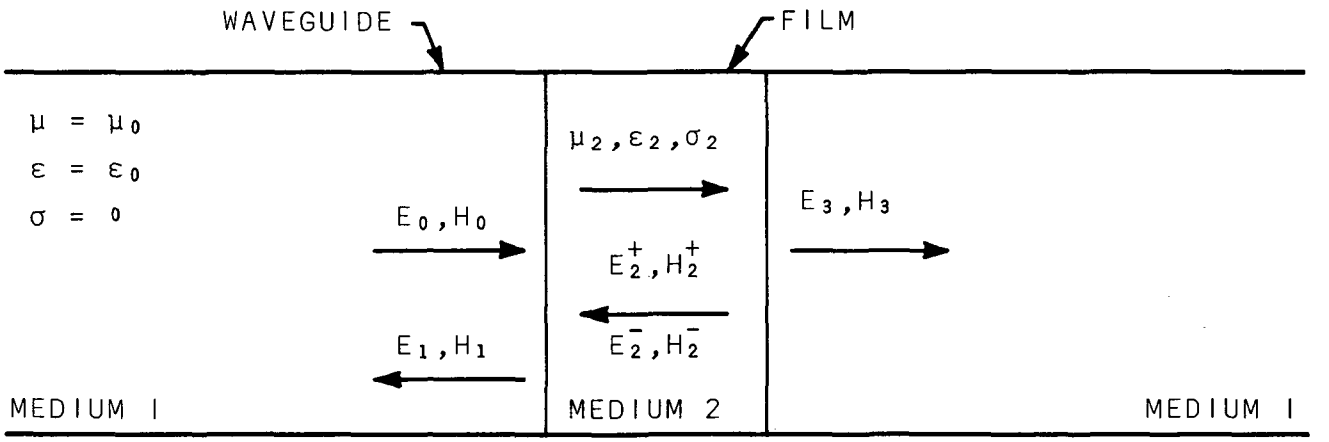

(B)

FIGURE 1. (A) FILM AND WAVEGUIDE ORIENTATION FOR BOUNDARY VALUE. (B) IDENTIFICATION OF FIELD COMPONENTS AND MEDIA PARAMETERS.

The power absorption coefficient is obtained from the fundamental expression:

$$A + R + T = 1 \tag{4}$$

In these expressions γ is the propagation factor and μ is the permeability of the film. The corresponding coefficients, γ_0 and μ_0, apply to the free space of the waveguide. The propagation coefficient for the film is

$$\gamma = [(\pi/a)^2 - \omega^2\mu\varepsilon + j\omega\mu\sigma]^{1/2} \tag{5}$$

where σ is the conductivity of the film and is a function of the film thickness. The permittivity of the film is ε, while ε_0 applies to free space. The waveguide width is a and ω is the angular frequency.

As a result of extensive experimental studies it was realized that the important parameter in these expressions is the product of the film conductivity, σ, times the film thickness, d. Ramey et al.[4] showed under the conditions $\gamma_0 d < 1$ and $\gamma d < 1$, the exponentials in Eq. (2) can be replaced by the first two terms of their MacLaurin series expansions. The transmission coefficient becomes:

$$T = \left| \frac{4(1+\gamma_0 d)}{[2-(\mu_0\gamma/\mu\gamma_0)-(\mu\gamma_0/\mu_0\gamma)](1-\gamma d)+[2+(\mu_0\gamma/\mu\gamma_0)+(\mu\gamma_0/\mu_0\gamma)](1+\gamma d)} \right|^2 \tag{6}$$

As $\gamma_0 \ll \gamma$ and $\gamma_0 d \ll 1$, Eq. (6) may be reduced to

$$T = \left|2/(2+\mu_0\gamma^2 d/\mu\gamma_0)\right|^2. \tag{7}$$

If the operating frequency is near the waveguide cutoff frequency, given by

$$f_c = \frac{1}{2a\sqrt{\mu_0\varepsilon_0}} \tag{8}$$

then[5,6] the power transmission coefficient is given by

$$T = \left|\frac{E_4}{E_0}\right|^2 = \left|\frac{2}{2 + \dfrac{\mu_0 \gamma^2 d}{\mu \gamma_0}}\right|^2 = \left|\frac{2}{2 + \dfrac{(\mu_0/\varepsilon_0)^{1/2}\sigma d}{[1 - (f_c/f)^2]^{1/2}}}\right|^2 \tag{9}$$

and the power reflection coefficient is given by

$$R_0 = \left|\frac{E_1}{E_0}\right|^2 = \left|\frac{\dfrac{\sqrt{\mu_0/\varepsilon_0}\ \sigma d}{2\sqrt{1 - (f_c/f)^2}}}{1 + \dfrac{\sqrt{\mu_0/\varepsilon_0}\ \sigma d}{2\sqrt{1 - (f_c/f)^2}}}\right|^2 = |r_0|^2 \tag{10}$$

Note that Eq. (10) is for the power reflected in the free space by the presence of the film. It does not apply to the internal reflections within the film. These reflections are taken into account in the derivation of these equations. Plots of Eqs. (9) and (10) are shown in Figs. 2 and 3. Experimental data points are also shown in Fig. 2. These data points all fall on or very close to the theoretical curve shown.

It should be emphasized that we are referring to the measured or actual conductivity of each film and not the technical bulk value. That is, in the manufacture of thin films it is difficult if not impossible to duplicate the electrical properties found in a normal bulk sample. Because of abnormal grain boundaries, dislocation, and other growth imperfections, the electron scattering mechanisms are greatly enhanced with resultant film conductivities running typically between $\frac{1}{4}$ and $\frac{1}{10}$ of the normal values found in the tables for bulk material.

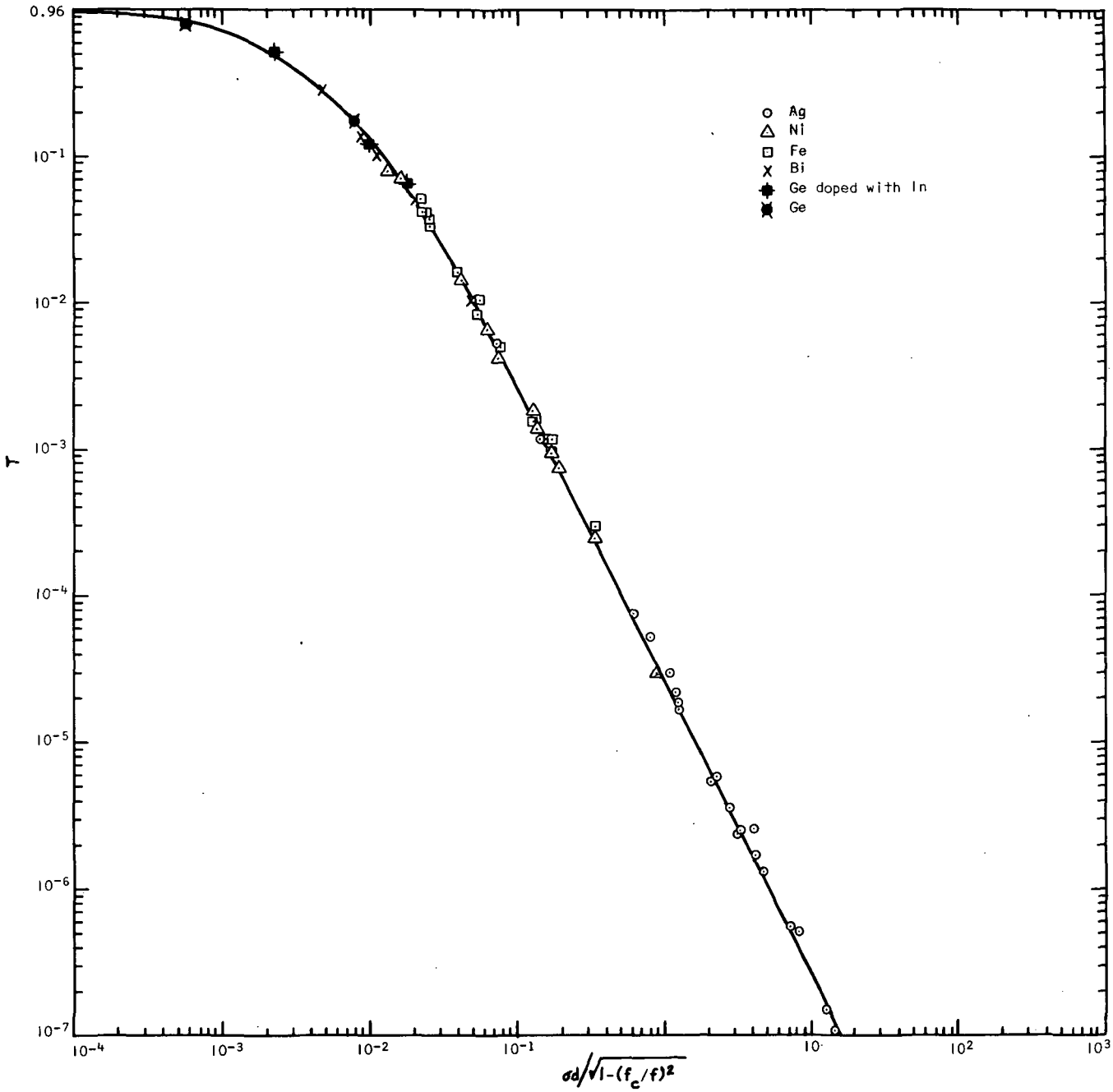

FIGURE 2. THE POWER TRANSMISSION OF THIN FILM WINDOWS IN WAVEGUIDE AS A FUNCTION OF σd.

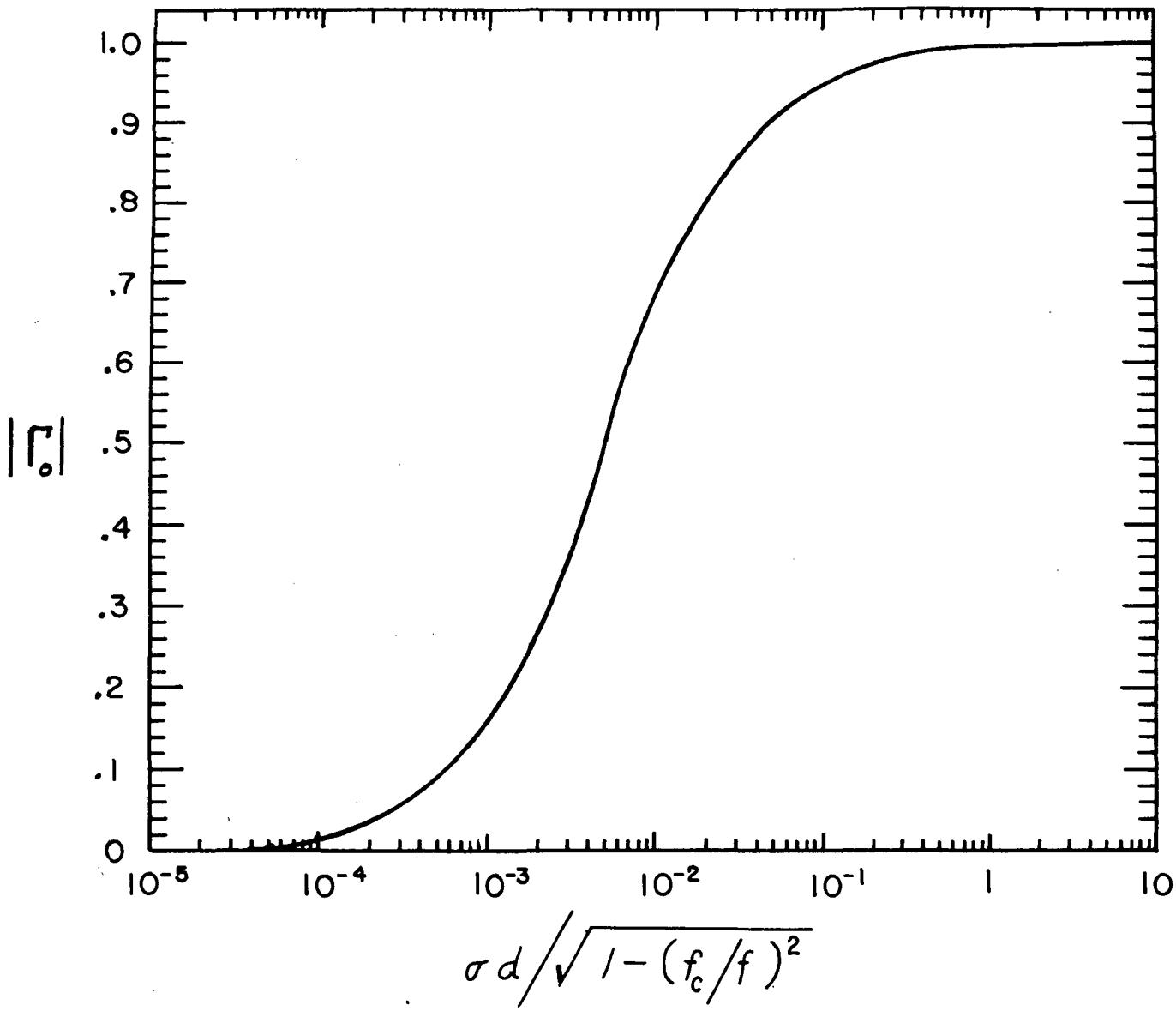

FIGURE 3. THE MAGNITUDE OF THE VOLTAGE REFLECTION COEFFICIENT FOR THIN FILM WINDOWS IN WAVEGUIDE.

SECTION II

THE ASYMMETRICAL IRIS

Although the thin film with $\sigma d < 10^{-3}$ is capable of transmitting over 95% of the incident power, it is somewhat more practical to use thicker metallic films with $\sigma d > 5 \times 10^{-3}$ and increase the transmitted power by placing an iris in the film. The use of symmetrical circular and elliptical irises has been covered in detail[5,6] by this NASA project. Asymmetrical rectangular irises or diaphragms are easily fabricated and lend themselves to electric control somewhat more readily than do the circular or elliptical irises. For this reason the rectangular iris has been used extensively in our research on horn antenna lobe slewing systems.

With reference to Fig. 4, the normalized susceptance presented by this asymmetrical iris is given approximately by[7]

$$B/Y_o = -\left(\frac{\lambda_g}{a}\right) \cot^2\left[\frac{\pi d}{2a}\left(1 + \csc^2 \frac{\pi d}{2a}\right)\right] \tag{11}$$

When $d = a/2$, then Eq. (11) reduces to

$$B/Y_o = -\lambda_g/a \tag{12}$$

where the guide wavelength is given by

$$\lambda_g = \frac{\lambda_0}{\sqrt{\frac{\varepsilon\mu}{\varepsilon_0\mu_0} - \left(\frac{\lambda_0}{\lambda_c}\right)^2}} \tag{13}$$

For a TE_{10}-mode, the cut-off wavelength, $\lambda_c = 2a$ and $\varepsilon \approx \varepsilon_0$, $\mu \approx \mu_0$ for and air-filled guide. Thus

$$B/Y_o = -\frac{\lambda_0}{a} \frac{1}{\sqrt{1 - (\lambda_c/2a)^2}} \tag{14}$$

$$= -1.71 \text{ (inductive)}$$

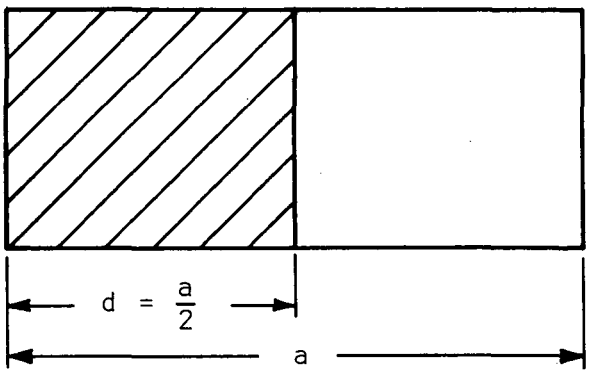

FIGURE 4. THE ASYMMETRICAL IRIS WITH d = a/2.

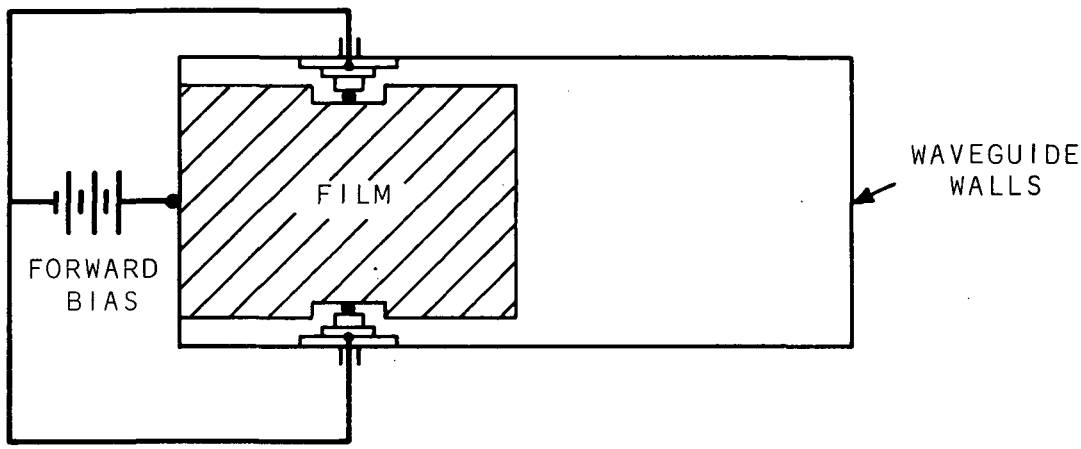

FIGURE 5. THE THIN FILM ASYMMETRICAL IRIS IS CONNECTED ELECTRICALLY TO THE LEFT-HAND WALL OF THE WAVEGUIDE. THE TOP AND BOTTOM OF THE FILM ARE EACH CONNECTED BY MEANS OF A MICROWAVE PIN DIODE TO THE UPPER AND LOWER WAVEGUIDE SURFACES.

or

$$X/Z_o = (B/Y_o)^{-1} = 0.585 \qquad (15)$$

With reference to Fig. 6, the thin nickel film shows a much greater variation of normalized reactance with respect to the total diode bias current (both diodes) than does a similar plate of stainless steel (bulk conductivity comparable to the nickel film). Although this iris is of the type that usually provides inductive reactance (Eq. (15), the presence of the diodes yields an overall capacitive reactance. As an example, for 0.5 ma bias current the net reactance of the thin film iris is -0.285 of which -0.255 is because of the thin film and -0.030 - 0.585 = -0.618 arises from the diodes. The associated normalized resistance of both of these irises is shown as a function of bias current in Fig. 7. The restricted electron transport mechanism in thin films results in the increased resistance of this type of iris as compared to the more conventional one. Phase shift as a function of bias current is shown in Fig. 8.

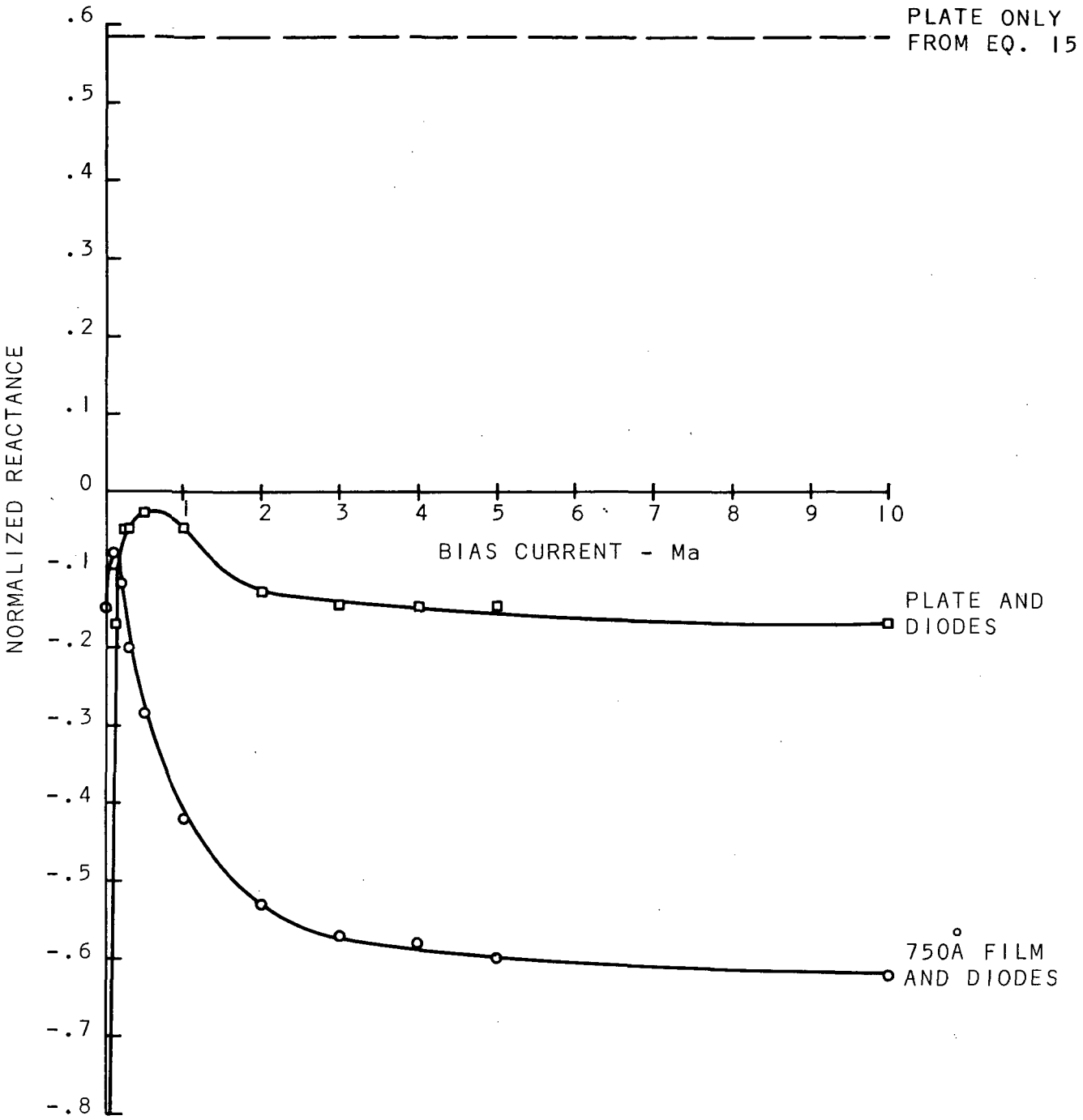

FIGURE 6. THE NORMALIZED REACTANCE OF A NICKEL FILM AND A STAINLESS STEEL PLATE AS A FUNCTION OF THE BIAS CURRENT TO BOTH DIODES.

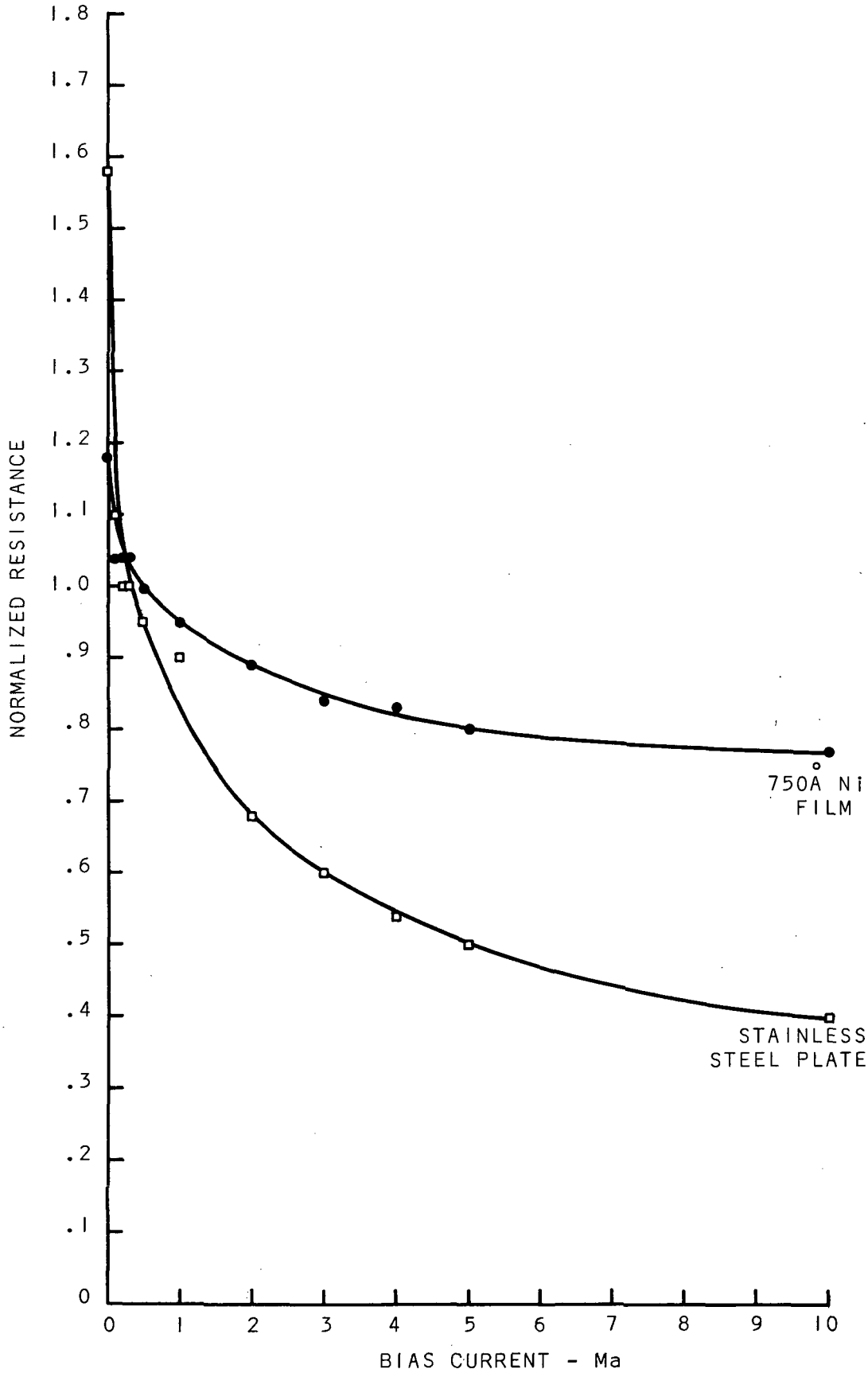

FIGURE 7. NORMALIZED RESISTANCE FOR THE IRIS CONFIGURATION DISCUSSED IN THE TEXT.

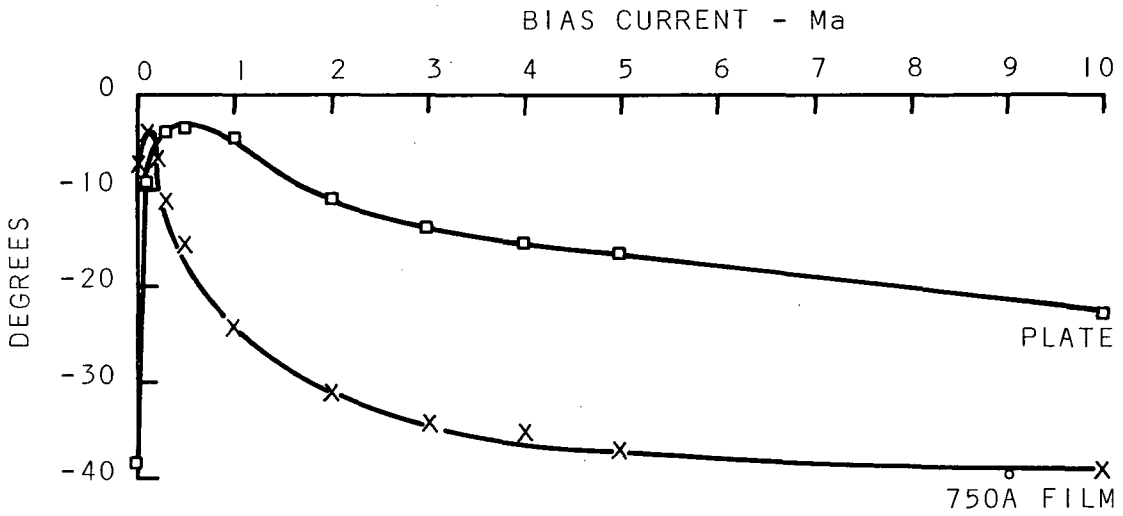

FIGURE 8. PHASE SHIFT AS A FUNCTION OF BIAS CURRENT.

SECTION III

ANTENNA BEAM-SLEWING

In the experimental work two and three horn antenna arrays at 9.8 GHz have been employed. An exact analysis of such an antenna system is difficult; however, point sources may be used in place of the horns and reasonable first order computations made. With reference to Fig. . the magnitude of the far field at a point P is easily shown to be[8]

$$E = [(1 - I \cos Z)^2 + I^2 \sin^2 Z]^{1/2} \qquad (16)$$

where the intensity of source number 2 is I times the intensity of source number 1. The angle Z is given by

$$Z = 2\pi * K * \cos A + D \qquad (17)$$

where the spacing between source 1 and source 2 is $2\pi K$ freespace wavelengths. The relative phase angle between the signal from each source is D. The polar angle about this antenna array is A.

Equations 16 and 17 are easily programmed in the BASIC computer language as shown in Figs. 10A and 10B. This program produces a teletype printer plot of 50 data points. The program was tested by (1) setting E = constant which should result in a circular plot. This is shown in Fig. 11 where we note the 2 to 1 elongation of the circle due to the line spacing being almost twice the character spacing on a line. (2) For half-wavelength spacing and a relative phase shift of 180 degrees the classical end-fire array shown in Fig. 12 is obtained. (3) For half-wavelength spacing and 0 degree relative phase shift the broadside pattern of Fig. 13 is obtained.

With these checks on the computer program, the horn spacing of 1.44 wavelengths, used in the laboratory, was fed into the program and the relative phase angle shifted from 5 to 30 degrees as this covers the range of phase shifts indicated in Fig. 8 for the thin film iris. The sequence of plots is shown in Figs. 14 through 19. The pattern consists

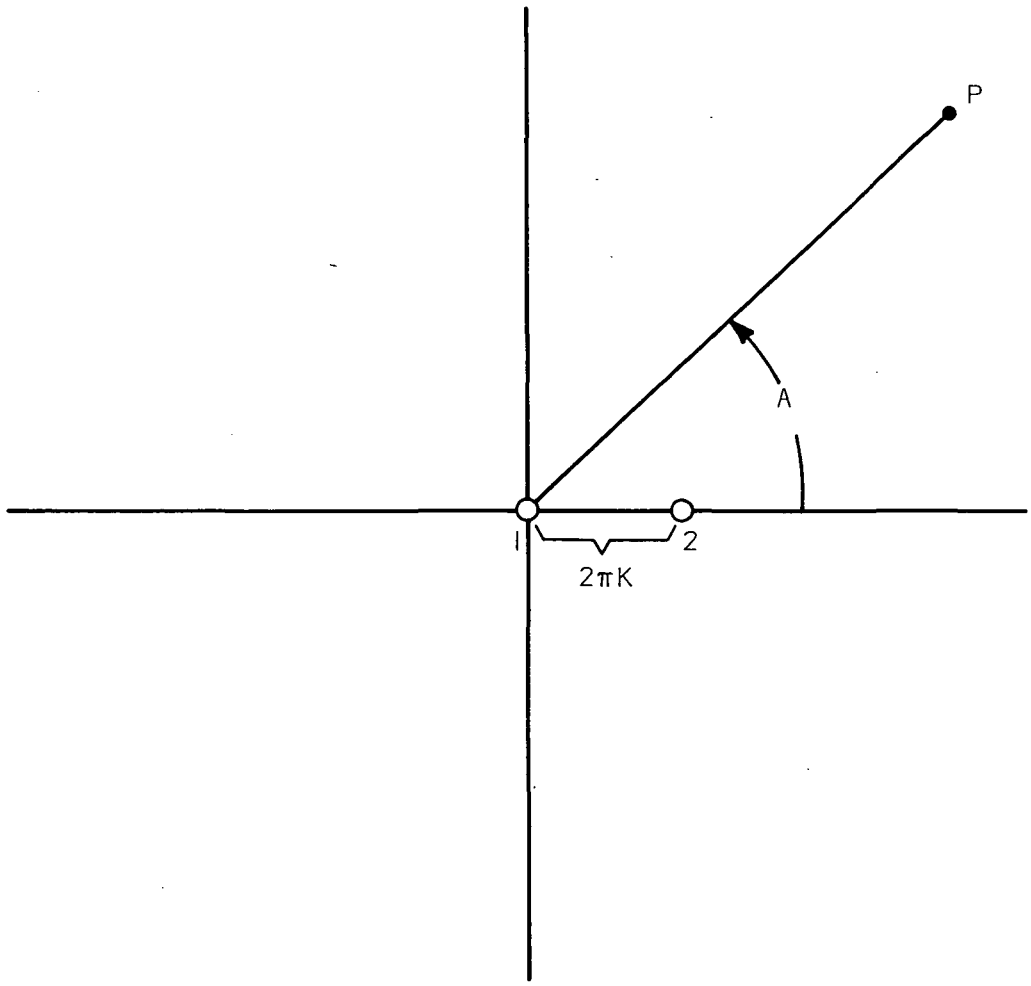

FIGURE 9. THE COMPUTATION OF THE ELECTRIC FIELD FROM TWO POINT SOURCES.

```
LIST

10  PRINT "POLAR PLOT OF E-FIELD FROM TWO POINT SOURCES"
20  PRINT "WHOSE RELATIVE PHASE ANGLE, D, IS THE VARIABLE"
30  PRINT "THE SOURCE SPACING IS 2*PI*K FREESPACE WAVELENGTHS"
35  DIM B[50]
40  DIM C[50]
50  DIM G[50]
60  DIM H[50]
65  READ K,N,I
66  PRINT "SOURCE NUMBER TWO I TIMES THE INTENSITY OF SOURCE ONE"
70  LET A2=6.2832/N
80  LET D2=(3.1416/180)*5
90  FOR D1=1 TO 6
100  LET F4=1
110  FOR A1=1 TO N
120  LET A=A1*A2
130  LET D=D1*D2
139  LET Z=6.2832*K*COS(A)+D
140  LET E=((1+I*COS(Z))↑2+I*I*(SIN(Z))↑2)↑.5
141  LET E=E/2
150  LET B[F4]=INT(25*E*COS(A))+25
160  LET C[F4]=INT(25*E*SIN(A))+25
170  LET F4=F4+1
180  NEXT A1
190  LET F4=F4-1
200  REM SORT C[F4] IN DECENDING ORDER AND B[F4] IN ASCENDING ORDER
320  MAT G=(1)*C
325  MAT H=(1)*B
330  FOR I1=1 TO F4
340  FOR I2=1 TO F4-1
350  IF C[I2]>C[I2+1] THEN 400
351  IF C[I2]<C[I2+1] THEN 360
352  IF B[I2] <= B[I2+1] THEN 400
360  LET G[I2]=C[I2+1]
365  LET H[I2]=B[I2+1]
370  LET G[I2+1]=C[I2]
375  LET H[I2+1]=B[I2]
380  LET C[I2]=G[I2]
385  LET B[I2]=H[I2]
390  LET C[I2+1]=G[I2+1]
395  LET B[I2+1]=H[I2+1]
400  NEXT I2
410  NEXT I1
420  REM BEGIN POLAR PLOT
430  FOR I4=1 TO 51
440  LET M=1
450  LET Y=51-I4
460  IF I4=26 THEN 620
470  FOR I3=1 TO N
480  IF Y <> C[I3] THEN 580
490  IF B[I3] >= 26 THEN 520
500  PRINT TAB(B[I3])"*";
510  GOTO 580
520  LET M=M+1
530  IF B[I3]=26 THEN 500
540  IF M>2 THEN 570
550  PRINT TAB(25)"!";TAB(B[I3])"*";
560  GOTO 580
```

FIGURE 10A. COMPUTER PROGRAM

```
570  PRINT TAB(B[I3])"*";
580  NEXT I3
590  IF M >= 2 THEN 640
600  PRINT TAB(25)"!"
610  GOTO 650
620  PRINT "*----*----*----*----*----0----*----*----*----*----*"
630  GOTO 650
640  PRINT
650  NEXT I4
660  PRINT
670  PRINT "RELATIVE PHASE ANGLE="D
680  PRINT
690  PRINT
700  PRINT
710  NEXT D1
720  DATA 1.44,50,1
730  END
```

FIGURE 10B. COMPUTER PROGRAM (CONTINUED)

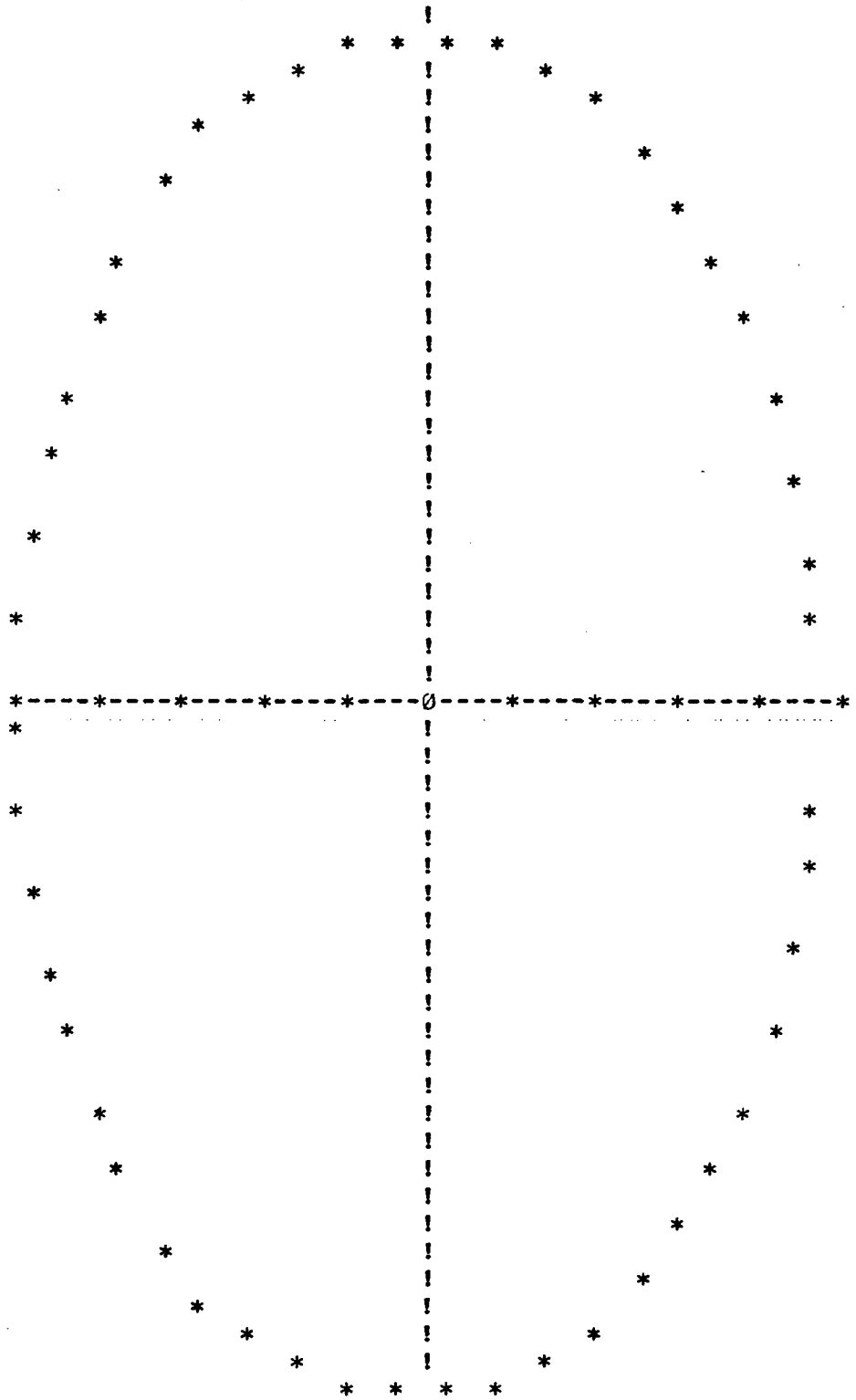

FIGURE 11. RESULT OF TEST OF PROGRAM FOR E = CONSTANT.

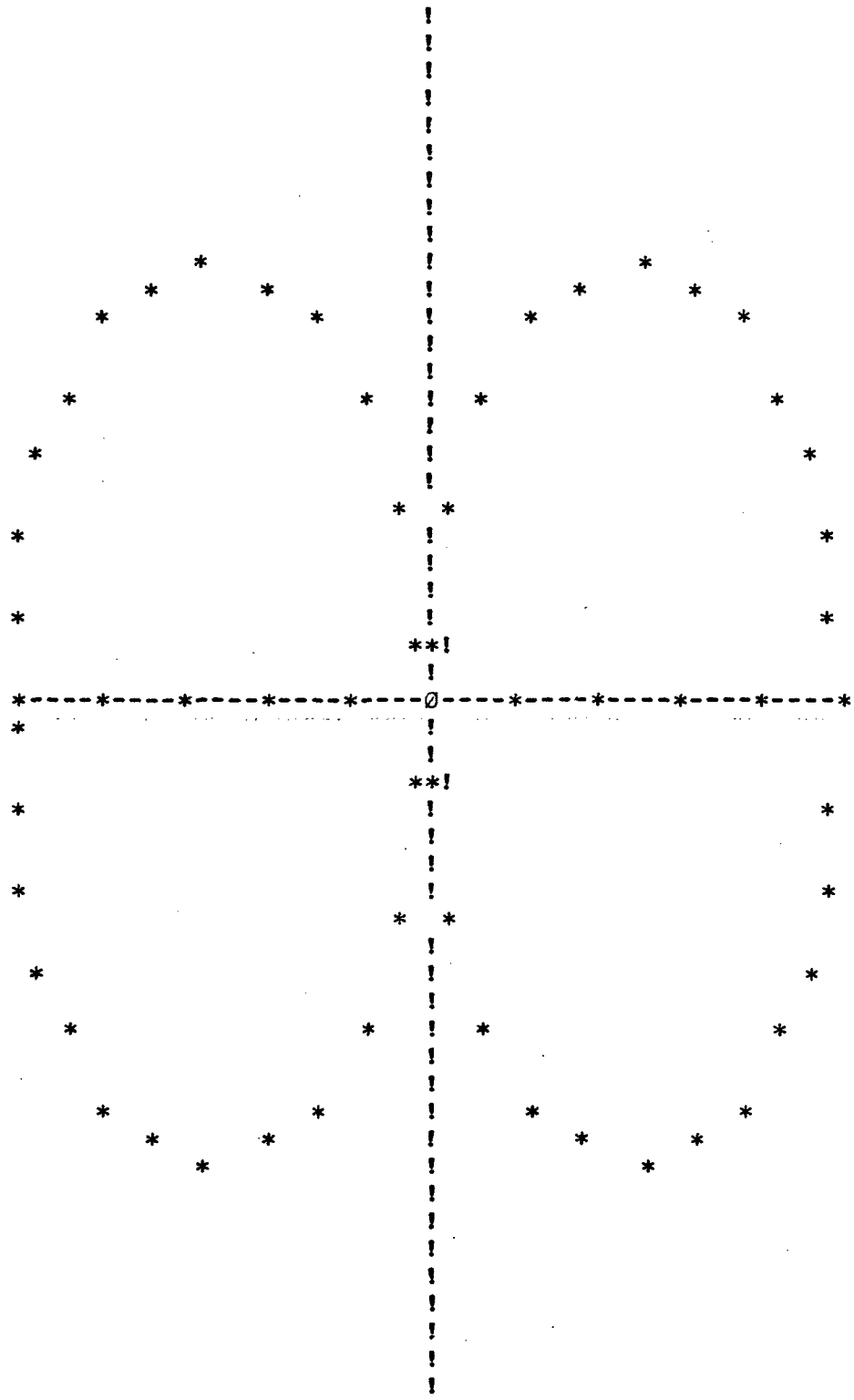

FIGURE 12. END-FIRE ANTENNA PATTERN.

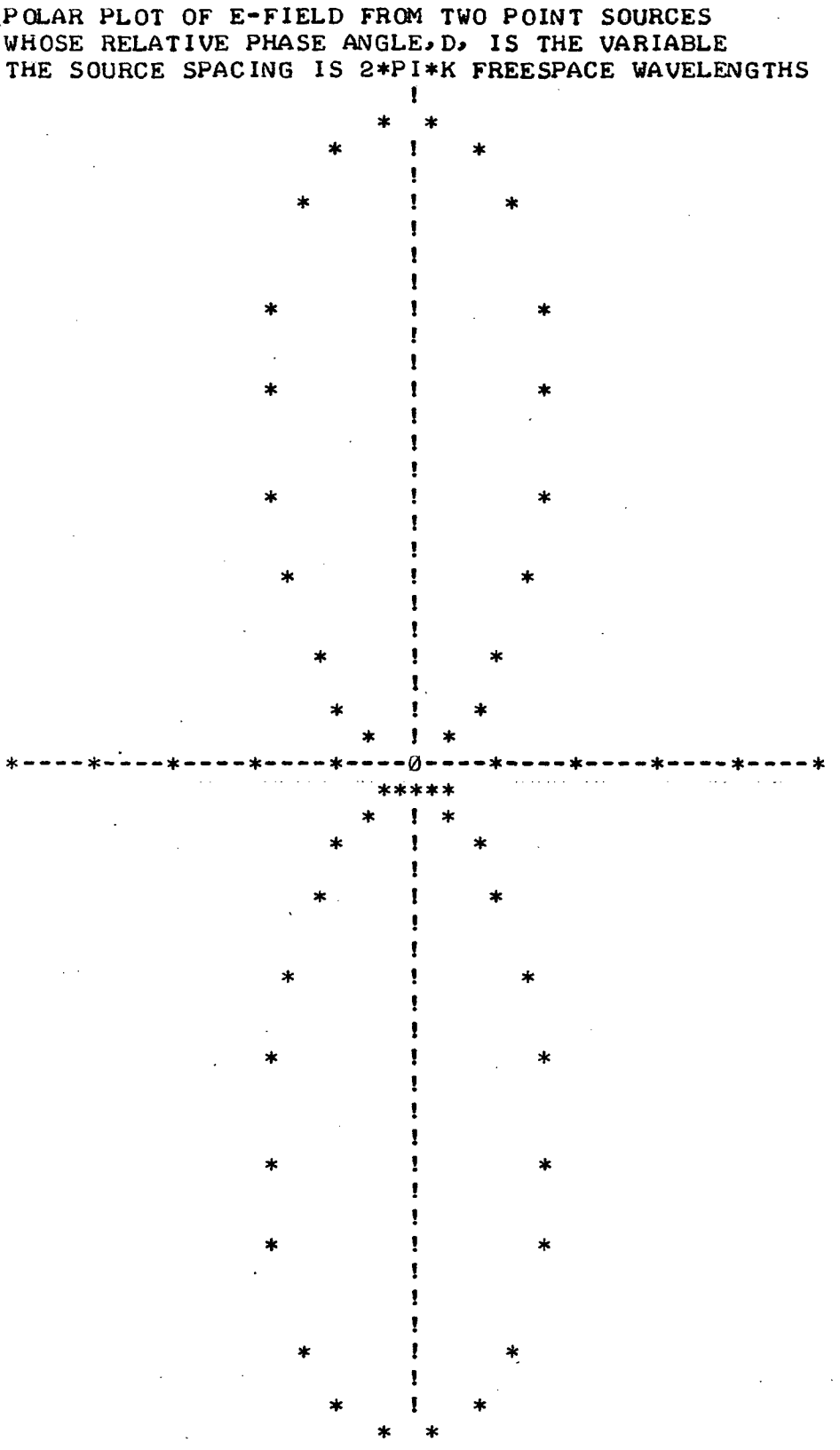

FIGURE 13. A BROADSIDE ANTENNA PATTERN.

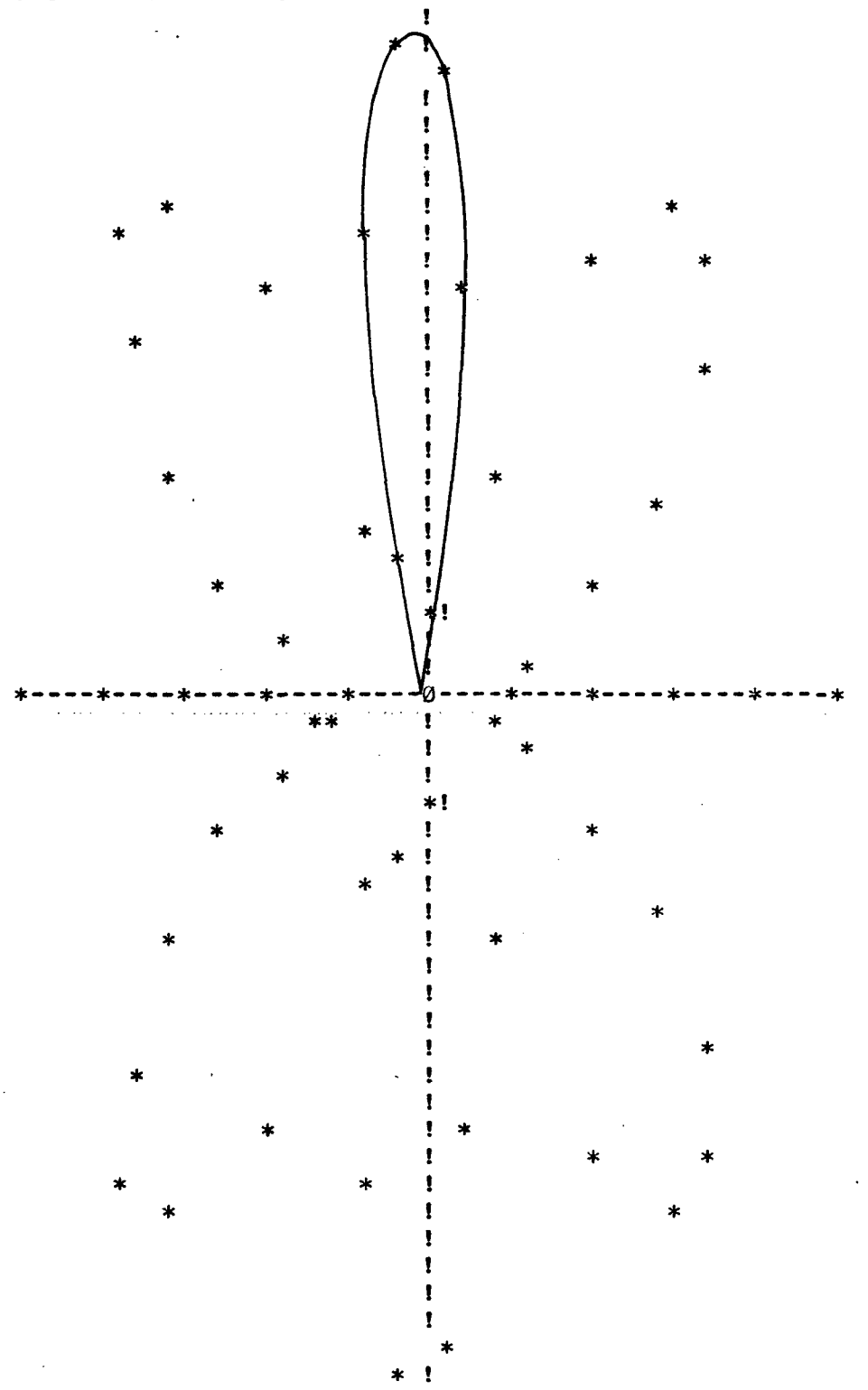

FIGURE 14. THE IDEALIZED TWO-HORN PATTERN (SKETCHED IN LOBE).

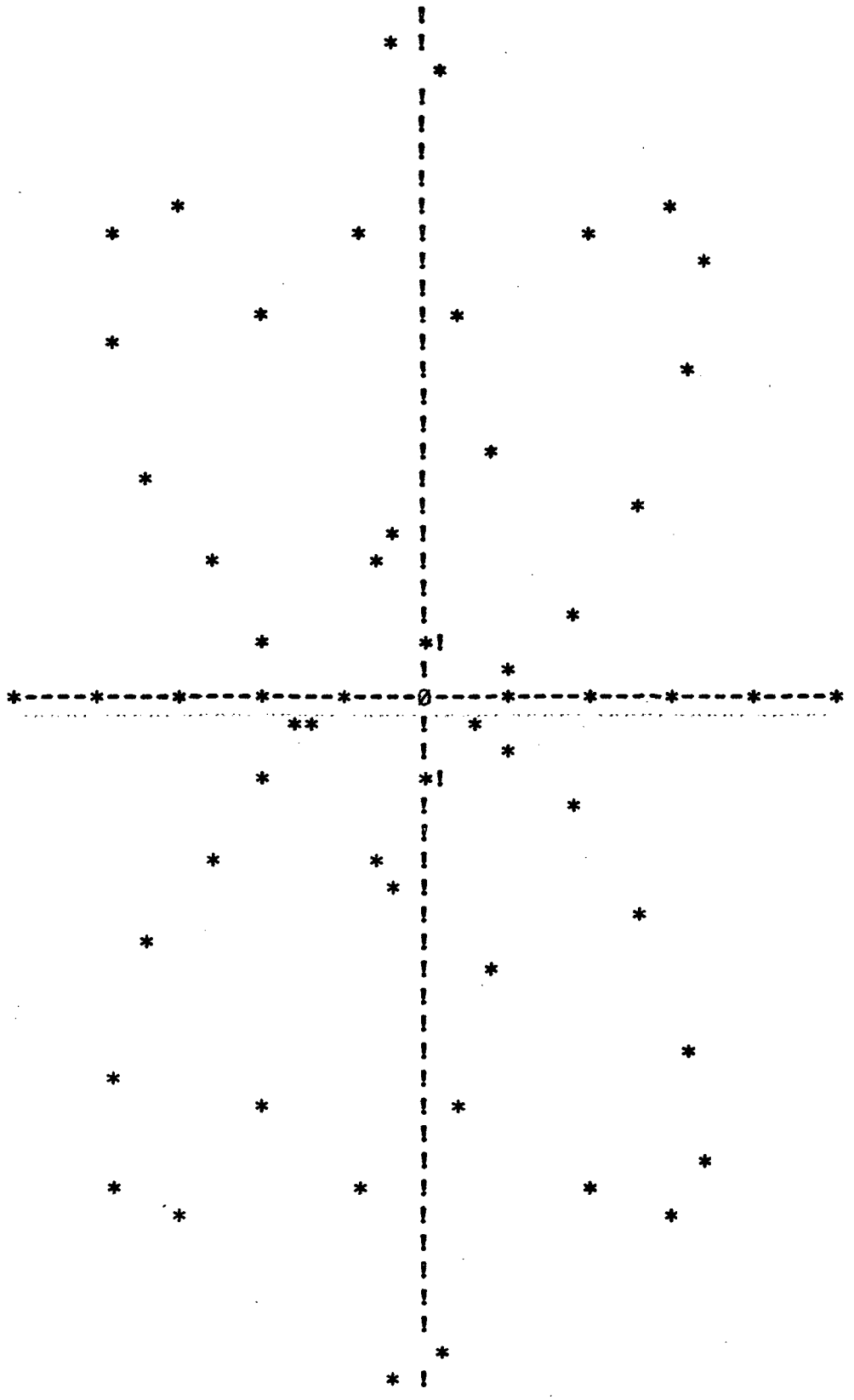

RELATIVE PHASE ANGLE= .174533

FIGURE 15. TWO-HORN PATTERN.

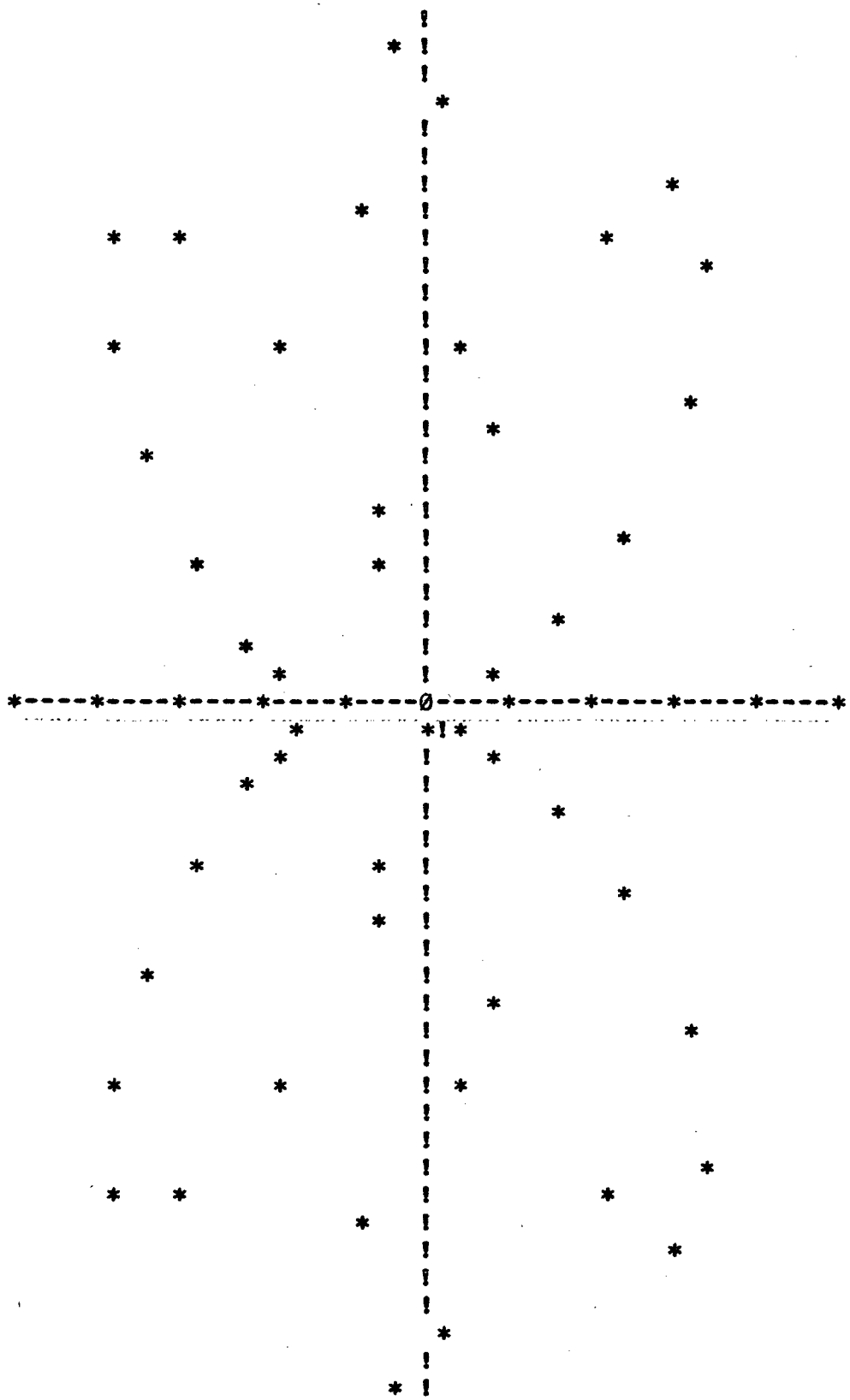

RELATIVE PHASE ANGLE= .2618

FIGURE 16. TWO-HORN PATTERN.

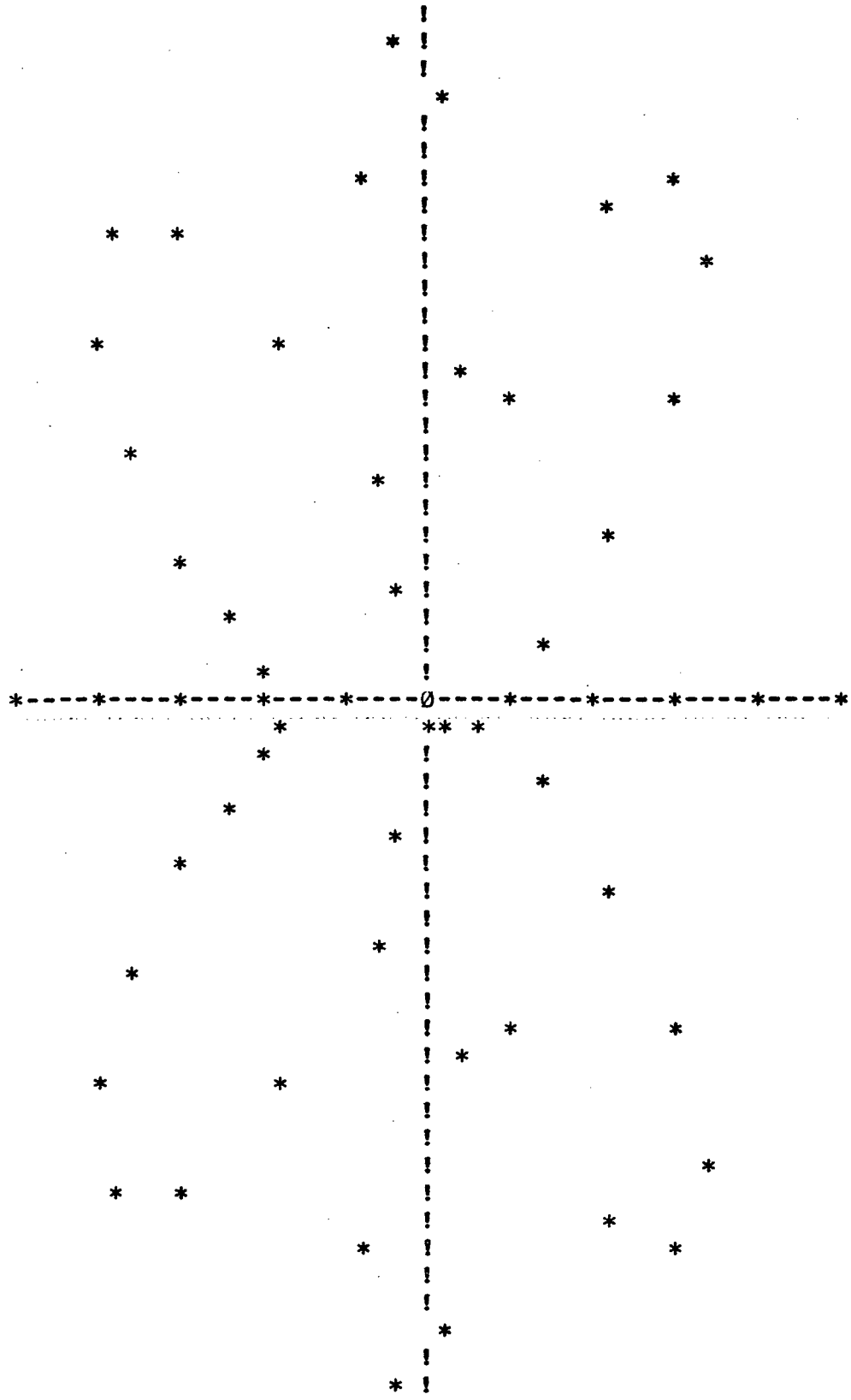

RELATIVE PHASE ANGLE= .349067

FIGURE 17. TWO-HORN PATTERN.

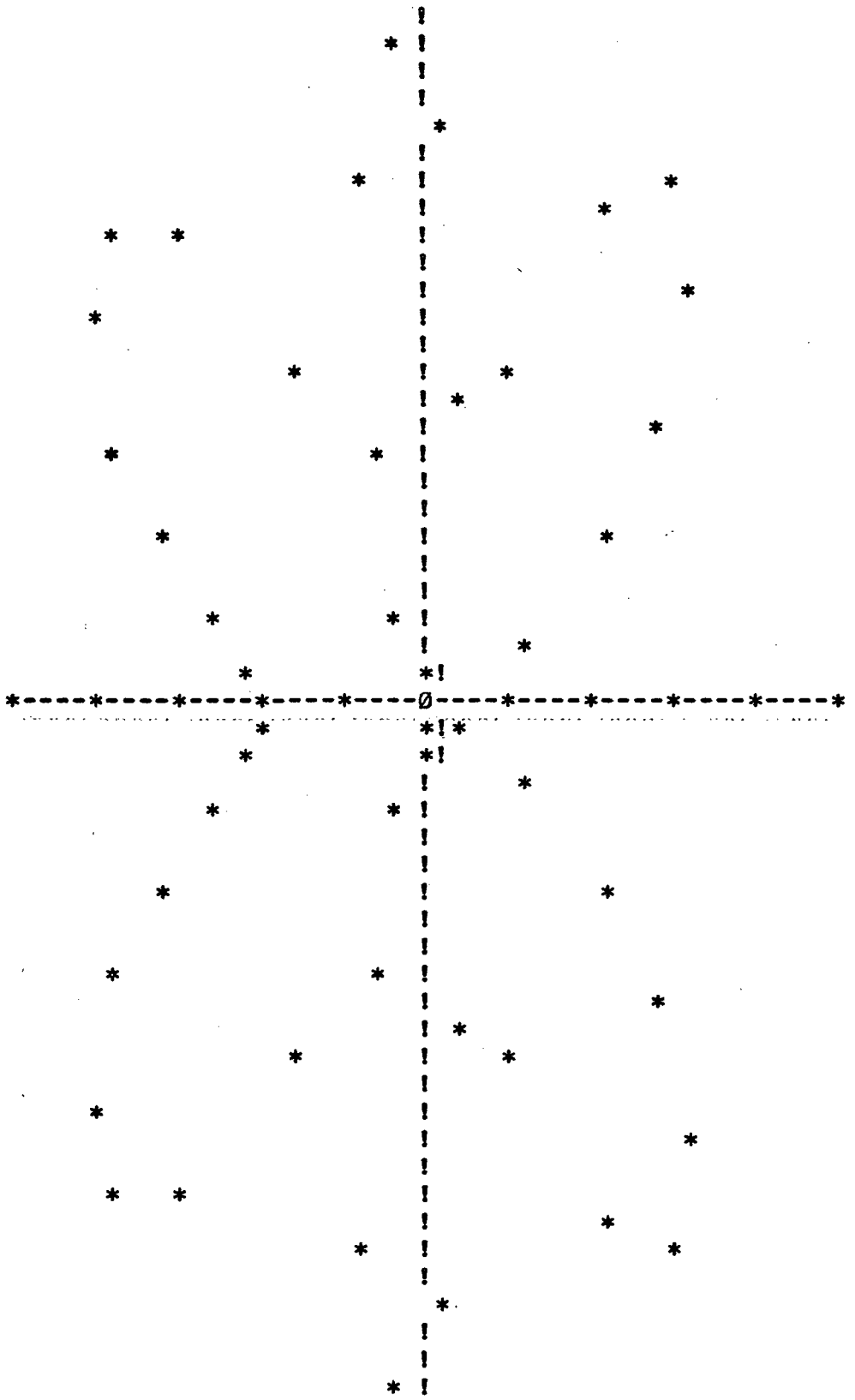

RELATIVE PHASE ANGLE= .436333

FIGURE 18. TWO-HORN PATTERN.

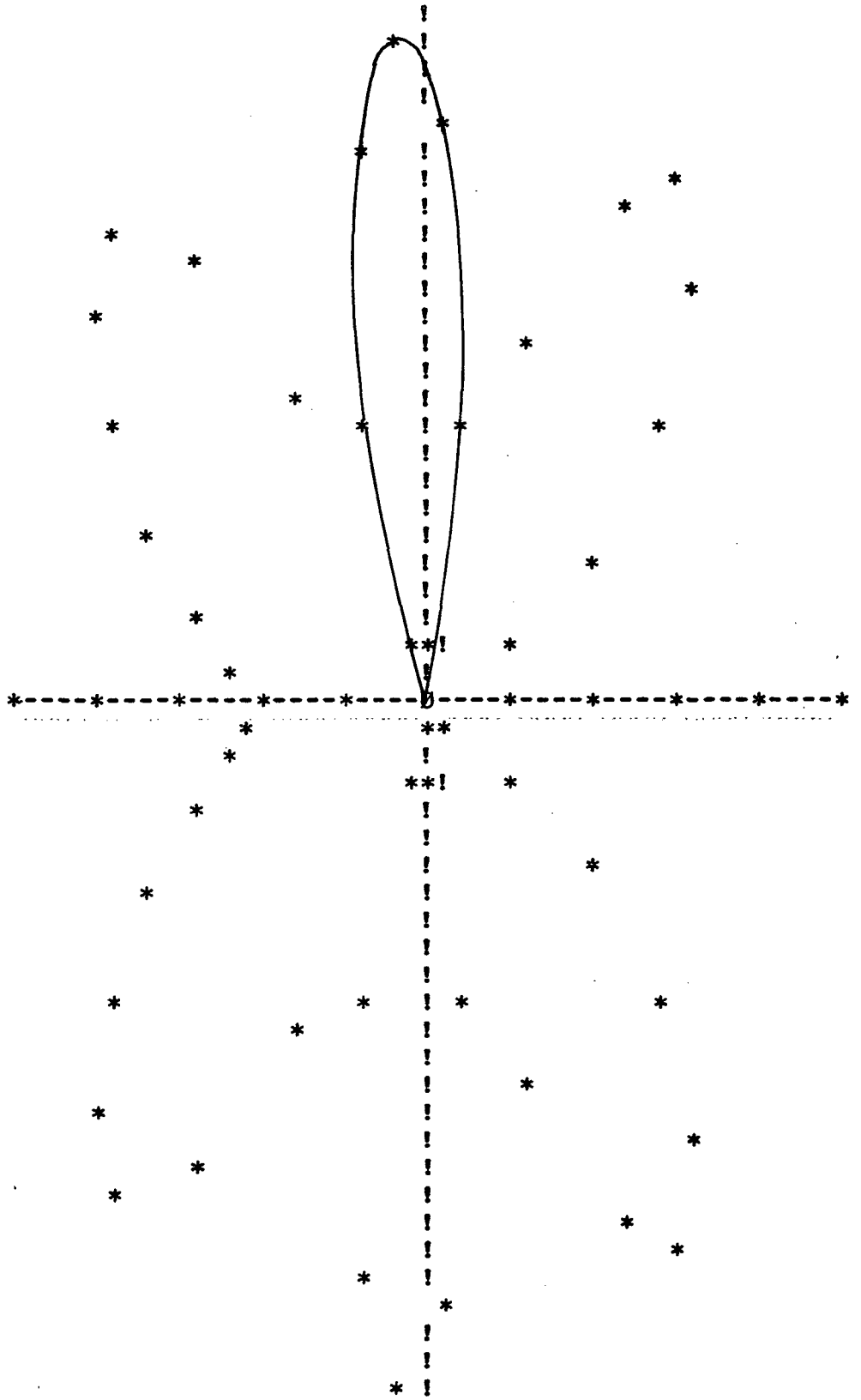

RELATIVE PHASE ANGLE= .5236

FIGURE 19. THE TWO-HORN ANTENNA LOBE (SKETCHED INDICATING A 3-DEGREE SLEW TO THE LEFT.

of six principal lobes and for zero relative phase shift the pattern is symmetrical about the x-axis. (Note that there appears to be an offset of one unit to the left of each pattern. This is simply roundoff error plus the quantizing effect of the teletype printer.)

The single lobe along the +y-axis represents the principal lobe from the actual two-horn antenna array employed in the slewing tests in the laboratory. If Fig. 14 is compared very carefully with Fig. 19, a 3-degree slew to the left is indicated. The fact that all of the lobes are being slewed to the left is easily noted.

Experimental verification of these theoretical computations was obtained using the laboratory arrangement shown in Fig. 20. The attenuators were adjusted so that the power from each horn was the same and the intensity pattern shown in Fig. 21 was recorded. The plot (Right) was obtained by applying bias to the film mounted in the feed line to the right-hand horn so that about 30° relative phase shift existed between the two horns. A receiving horn travelling on an arc of about 11.7 feet was used to detect the signal. The film in the left hand horn was at zero bias during this run. The situation was then reversed with bias applied to the thin film iris in the feed line to the left-hand horn and zero bias on the right-hand film. The plot marked (Left) was then obtained.

The difference between the peaks is 5.2 degrees for a full slew or 2.6 degrees for a slew to one side of center. This compares very favorably with the slew of about 3 degrees indicated by Fig. 19 from the computer plot. A three horn antenna was also tested in a similar manner. The center horn was direct feed (no iris). The results are shown in Fig. 22 with a total slew of about 3.8 degrees.

Thus, the thin film iris is capable of providing the necessary phase shift for practical antenna array slewing.

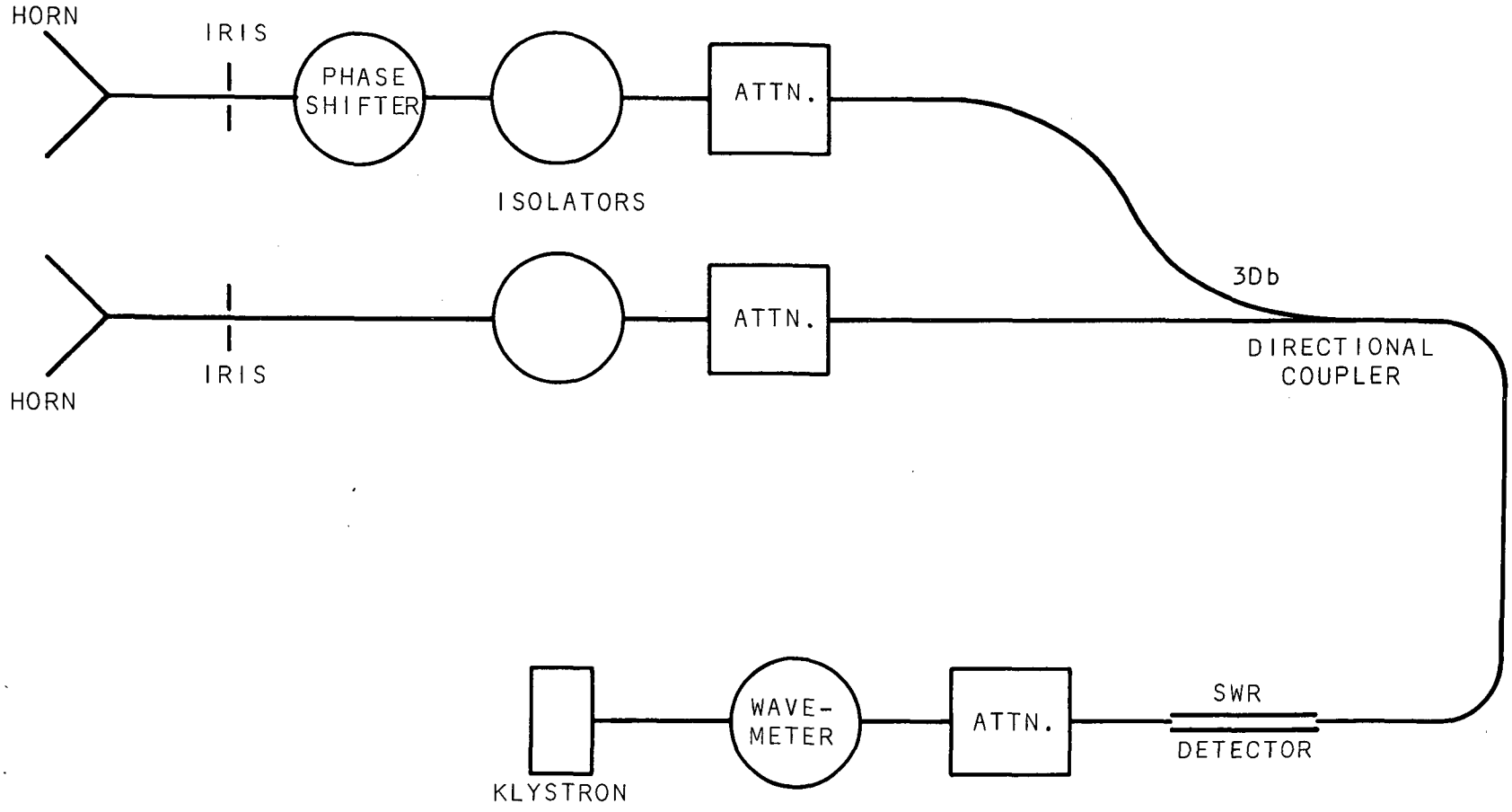

FIGURE 20. THE 9.8 GHz EXPERIMENTAL ARRANGEMENT FOR STUDYING THE SLEWING OF A SIMPLE HORN ANTENNA ARRAY.

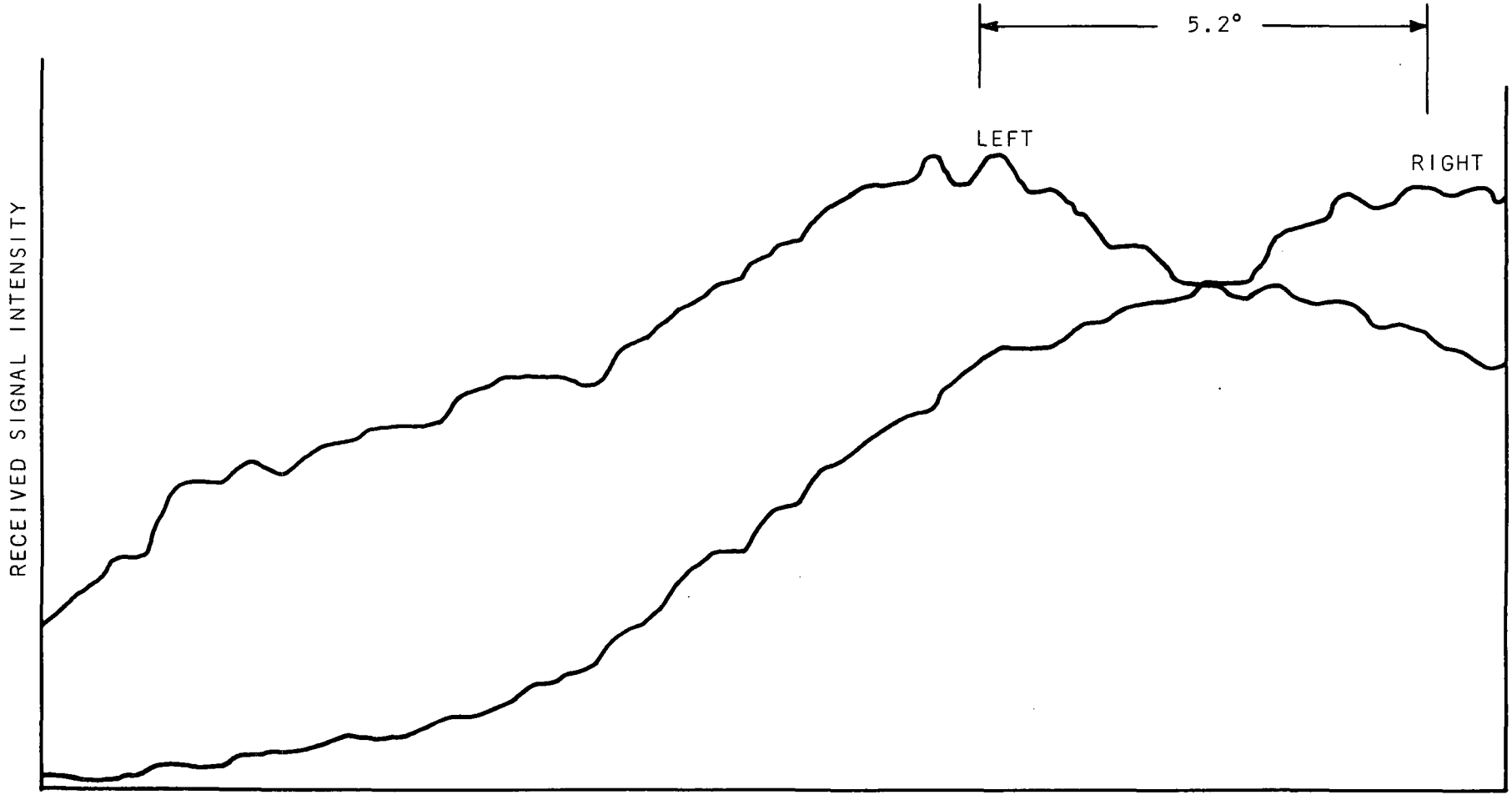

FIGURE 21. SLEWING BY THIN FILM IRISES OF A TWO-HORN 9.1 GHz ANTENNA. HORN SPACING WAS 1.44 λ_0

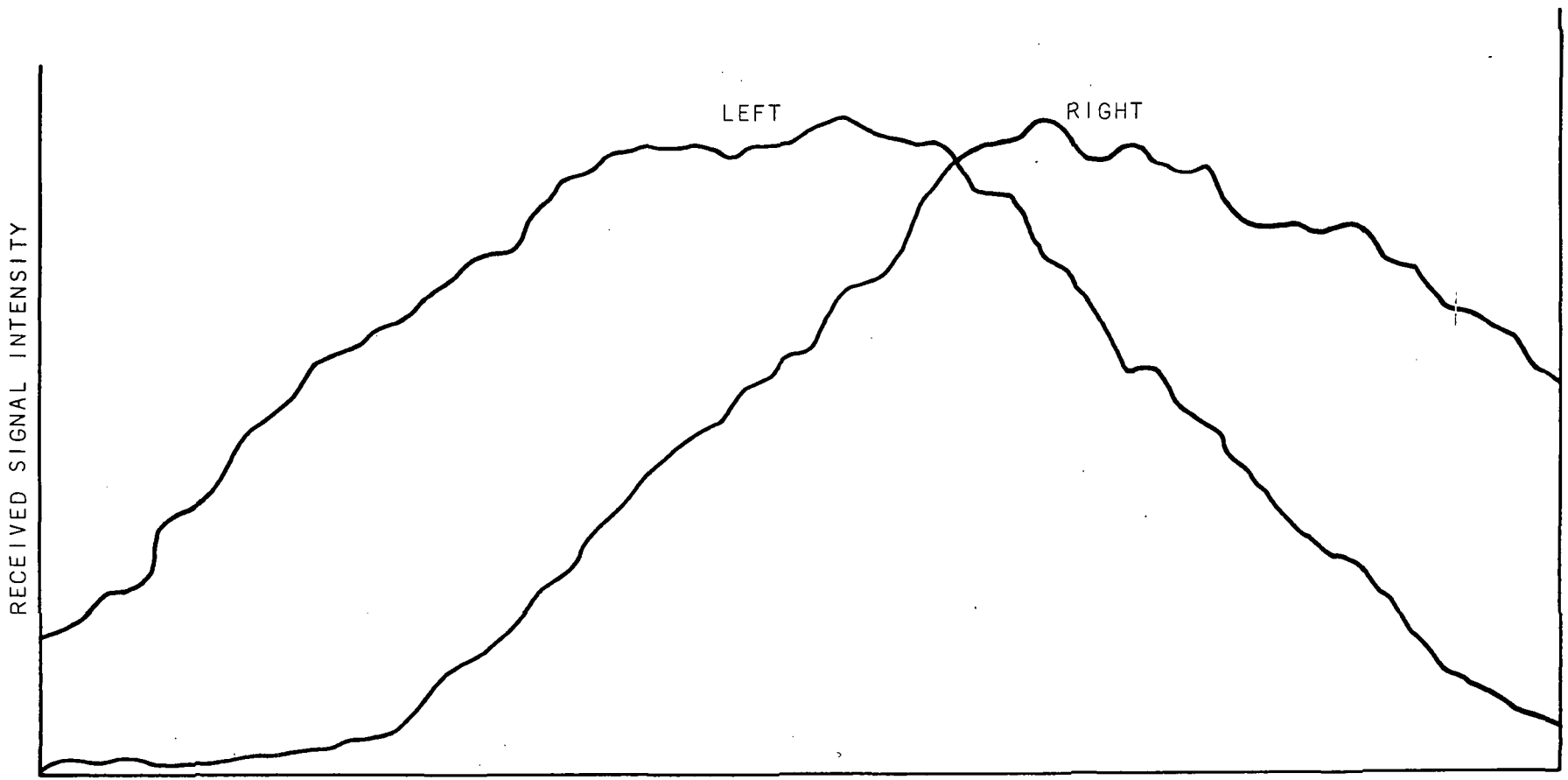

FIGURE 22. TESTS ON THE SLEWING BY THIN FILM IRISES OF A THREE-HORN ANTENNA ARRAY AT 9.8 GHz

SECTION IV

CRYOGENIC STUDIES

A part of this research effort was directed at studies of the reactance of the thin film iris under superconducting conditions. This effort has been plagued by repeated problems from the reduced research budget (50%) to equipment abnormalities. A Sulfrian brand cryostat with a 20 GHz tail piece was purchased and all associated equipment, including a helium return line to our physics department (where our He is obtained) installed. Testing began in the fall of 1970. The present status is that there appears to be a leak in the cryostat which appears when the liquid helium is inserted but which cannot be detected with a helium leak detector under normal conditions. We have worked on this problem for four months since the expiration of the contract support. Further unsupported effort on the cryostat problem is not feasible at this time.

REFERENCES

1. Kaplan, A. E., Radiotekhnika i Elektronika, 9, 1781 (1964)

2. Korolev, F. A., and Gridnev, V. I., Radiotekhnika i Elektronika, 10, 1718 (1965).

3. Ramey, R. L., and Lewis, T. S., J. of Appl. Phys., 39, 1747-1752 (1968).

4. Ramey, R. L., Kitchen, W. J., Loyd, J.M., and Landes, H. S., J. of Appl. Phys., 39, 3883-3884 (1968).

5. Ramey, R. L., Landes, H. S., and Manus, E. A., NASA CR-1364, June 1969.

6. Ramey, R. L., Landes, H. S., and Manus, E. A., IEEE Trans, on Microwave Theory and Technique, MTT-18, No. 4, 196-204, April, 1970.

7. Montgomery, C. G., Dicke, R. H., and Purcell, E. M., Principles of Microwave Circuits, MIT RAdiation Lab. Series, pg. 165, McGraw-Hill Book Co., New York (1948).

8. Krans, J. D., Antennas, pg. 65, McGraw-Hill Book Co., New York (1950).

DISTRIBUTION LIST

Copy No.	
1 - 5	National Aeronautics and Space Administration Office of Scientific and Technical Information (Code US) Washington, D. C. 20546
6 - 7	National Aeronautics and Space Administration Flight Instrumentation Division Langley Research Center Hampton, Virginia 23365
8	C. B. Thomas
9 - 10	R. L. Ramey
11	L. T. Rader
12 - 13	R. H. Austin Science/Technology Information Center
14 - 20	RLES Files